Spontaneous Inversion Symmetry Breaking and Emergence of Berry Curvature and Orbital Magnetization in Topological $ZrTe_5$ Films

Erqing Wang,[1] Hui Zeng,[2] Wenhui Duan,[2,3,4,5] and Huaqing Huang[1,5,6,*]
[1]School of Physics, Peking University, Beijing 100871, China
[2]State Key Laboratory of Low-Dimensional Quantum Physics, Department of Physics, Tsinghua University, Beijing 100084, China
[3]Institute for Advanced Study, Tsinghua University, Beijing 100084, China
[4]Frontier Science Center for Quantum Information, Beijing 100084, China
[5]Collaborative Innovation Center of Quantum Matter, Beijing 100871, China
[6]Center for High Energy Physics, Peking University, Beijing 100871, China

(Received 13 December 2023; revised 4 April 2024; accepted 21 May 2024; published 28 June 2024)

$ZrTe_5$ has recently attracted much attention due to the observation of intriguing nonreciprocal transport responses which necessitate the lack of inversion symmetry ($\mathcal{I}$). However, there has been debate on the exact $\mathcal{I}$-asymmetric structure and the underlying $\mathcal{I}$-breaking mechanism. Here, we report a spontaneous $\mathcal{I}$ breaking in $ZrTe_5$ films, which initiates from interlayer sliding and is stabilized by subtle intralayer distortion. Moreover, we predict significant nonlinear anomalous Hall effect (NAHE) and kinetic magnetoelectric effect (KME), which are attributed to the emergence of Berry curvature and orbital magnetization in the absence of $\mathcal{I}$ symmetry. We also explicitly manifest the direct coupling between sliding ferroelectricity, NAHE, and KME based on a sliding-dependent $k \cdot p$ model. By studying the subsurface sliding in $ZrTe_5$ multilayers, we speculate that surface nonlinear Hall current and magnetization would emerge on the natural cleavage surface. Our findings elucidate the sliding-induced $\mathcal{I}$-broken mechanism in $ZrTe_5$ films and open new avenues for tuning nonreciprocal transport properties in Van der Waals layered materials.

DOI: 10.1103/PhysRevLett.132.266802

Introduction.—Zirconium pentatelluride $ZrTe_5$ is a versatile topological material that has attracted broad interest. Previous theoretical and experimental studies have uncovered various novel quantum phenomena of $ZrTe_5$, such as giant resistivity anomaly [1–4], large anomalous Hall effect (AHE) [5–10], three-dimensional (3D) quantum Hall effect [11–13], chiral magnetic effect [14,15], exotic thermoelectric response [16–20], and diverse topological phase transitions driven by various external stimuli, such as temperature [21–25], strain [26–28], light [29–32], and Zeeman field [33–37]. The emergence of these fascinating phenomena reflects the characterization of distinct phases of $ZrTe_5$. In contrast, the recently observed gigantic magnetochiral anisotropy [38], nonlinear anomalous Hall effect (NAHE) [39], and circular photogalvanic effect [40], which all necessitate the lack of inversion symmetry ($\mathcal{I}$) [41,42], have brought intense debates on the exact lattice structure and crystal symmetry of the $\mathcal{I}$-asymmetric phase of $ZrTe_5$. In particular, the specific $\mathcal{I}$-breaking modes and their underlying mechanism have remained elusive.

On the other hand, the reduction of dimensionality brings up more intriguing properties that are unique relative to their bulk counterpart [43,44]. For example, few-layer $ZrTe_5$ is actively investigated due to the emergent large-gap quantum spin Hall effect [45–47], giant optical and electric anisotropy [48,49] that may be promising for quantum device applications. More importantly, quasi-2D thin films with Van der Waals (vdW) layered structures also enable markedly different $\mathcal{I}$-breaking mechanisms, allowing for the emergence of interlayer sliding ferroelectricity [50–56], electrically switchable NAHE [57–62], and kinetic magnetoelectric effect (KME) that generates a net magnetization by an electric current [63–65]. Although broken $\mathcal{I}$ symmetry is a prerequisite for these effects, the corresponding electric polarization, nonlinear anomalous Hall current, and current-induced magnetization depend sensitively on the degree of asymmetry and are clearly correlated to each other, as shown in this Letter.

In this Letter, we report that a spontaneous $\mathcal{I}$ symmetry breaking occurs in thin films of $ZrTe_5$ which originates from interlayer sliding and subtle intralayer distortion. Taking trilayer $ZrTe_5$ as an example, we show the existence of sliding ferroelectricity where two $\mathcal{I}$-related polar phases exhibit sizable in-plane electric polarization, and the low energy barrier along the polarity reversal path enables ultrafast ferroelectric switching via low voltage. Remarkably, the sliding-initiated $\mathcal{I}$ breaking also induces prominent distributions of Berry curvature (BC) and orbital magnetization (OM), which gives rise to a significant NAHE and KME that are controllable by sliding ferroelectricity. In addition, we discuss the role of subsurface sliding on these effects in multilayers and argue that the natural cleavage surface leads to the manifestation of a surface nonlinear Hall current and magnetization solely arising due to the local spontaneous symmetry breaking at the surface.

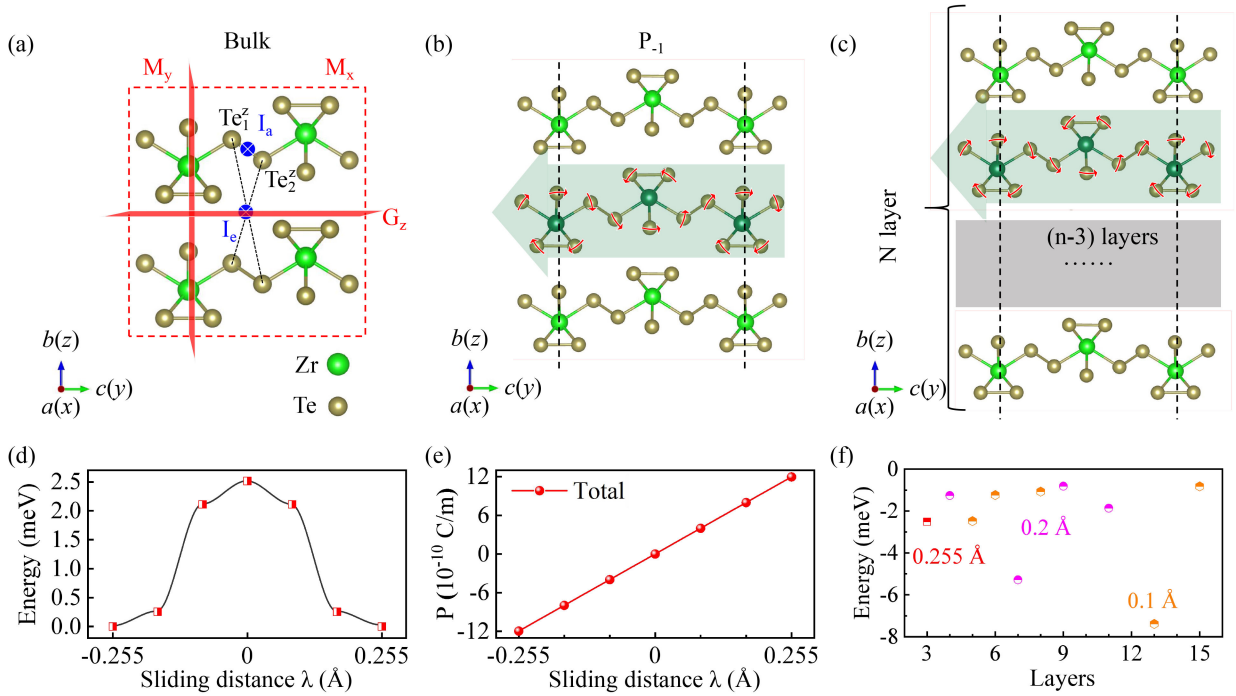

FIG. 1. (a) Atomic structure of bulk $ZrTe_5$ where the intralayer and interlayer inversion centers (I_a and I_e) are marked by blue dots. The mirror ($\mathcal{M}_x$ and $\mathcal{M}_y$) and glide mirror plane $\mathcal{G}_z$ are colored in red. (b) Slide structure (P_{-1}) of trilayer $ZrTe_5$ (formed by an overall interlayer sliding of the middle layer (light green arrow) and subtle intralayer distortions (red arrows). (c) Illustration of subsurface sliding in multilayer $ZrTe_5$ slab cut from the bulk. (d) Energy profiles for ferroelectric switching of trilayer $ZrTe_5$. (e) Variation of in-plane electric polarization under ferroelectric switching from P_{-1} to P_1. (f) Change in energy versus the numbers of layers in slide $ZrTe_5$ films [as illustrated in (c)] with different optimal sliding displacement λ coloring the same as corresponding marker dots.

Noncentrosymmetric polar trilayer structures.—Bulk $ZrTe_5$ crystallizes in an orthorhombic layered structure with space group *Cmcm*, where 2D layers stack in the AB sequence along the *b* axis and interact via weak vdW interactions [66], as shown in Fig. 1(a). For each layer in the *a*-*c* plane, trigonal prismatic chains of $ZrTe_3$ along the *a* axis are connected by the adjacent zigzag chains of $Te^z_{1,2}$ atoms [45]. Bulk $ZrTe_5$ is centrosymmetric with two inversion centers (I_a and I_e), which are located at the intralayer $Te^z_{1,2}$ bond and interlayer space, respectively. Our first-principles calculations show that previously proposed $\mathcal{I}$-breaking modes (e.g., staggered displacements of adjacent $Te^z_{1,2}$ chains [38]) are energetically unfavorable [see Fig. S2 and Tables S1 and S2 in Supplemental Material (SM) [67]]. Because of these inversion centers, prototypical $ZrTe_5$ multilayers are also centrosymmetric without any polarizations. Given that the interlayer sliding cannot break $\mathcal{I}$ in the bilayer as well as the bulk $ZrTe_5$, we first consider the trilayer $ZrTe_5$, which is the minimum system for studying interlayer sliding-induced $\mathcal{I}$ breaking.

For trilayer $ZrTe_5$, the initial ABA-stacked configuration cut from the bulk belongs to space group *Pmmn* and is centrosymmetric nonpolar, which serves as a hypothetical reference phase P_0. After structural optimization based on first-principles calculations [67], we find two stable noncentrosymmetric polar structures with space group $Pmn2_1$, which are related by a spatial inversion. We, therefore, label them as P_1 and P_{-1}, one of which is shown in Fig. 1(b). Detailed atomic structural analysis indicates that they are initiated by interlayer sliding of the middle layer by a distance of 0.255 Å along the *c* axis (green arrow) and accompanied by subtle intralayer distortions composed of alternative clockwise and counterclockwise twist of alternating $ZrTe_5$ pentagons (red arrows), as shown in Fig. 1(b). Noticeably, in bulk $ZrTe_5$, such twisted crystal lattice motion corresponds to the dynamic $\mathcal{I}$ breaking induced by light [40], but spontaneously happens in thin films of $ZrTe_5$. More importantly, we found an increase in the total energy if we only continuously varied degrees of interlayer sliding from the initial configuration but without structural relaxation to accomplish intralayer distortion. In contrast, the intralayer distortion offsets the energy increase which ultimately stabilizes the sliding structure (see Fig. S9 in SM [67]). Therefore, the subtle intralayer distortion plays an important role in the spontaneous $\mathcal{I}$ breaking.

Spontaneous polarization and sliding ferroelectricity.—Interestingly, spontaneous electric polarizations emerge in both noncentrosymmetric trilayer structures. Because of the existence of mirror $\mathcal{M}_x$ and glide mirror $\mathcal{G}_z = (\mathcal{M}_z|1/2, 1/2, 0)$ symmetries, the nonzero component of polarization is aligned along the *c* axis (*y* direction). Our

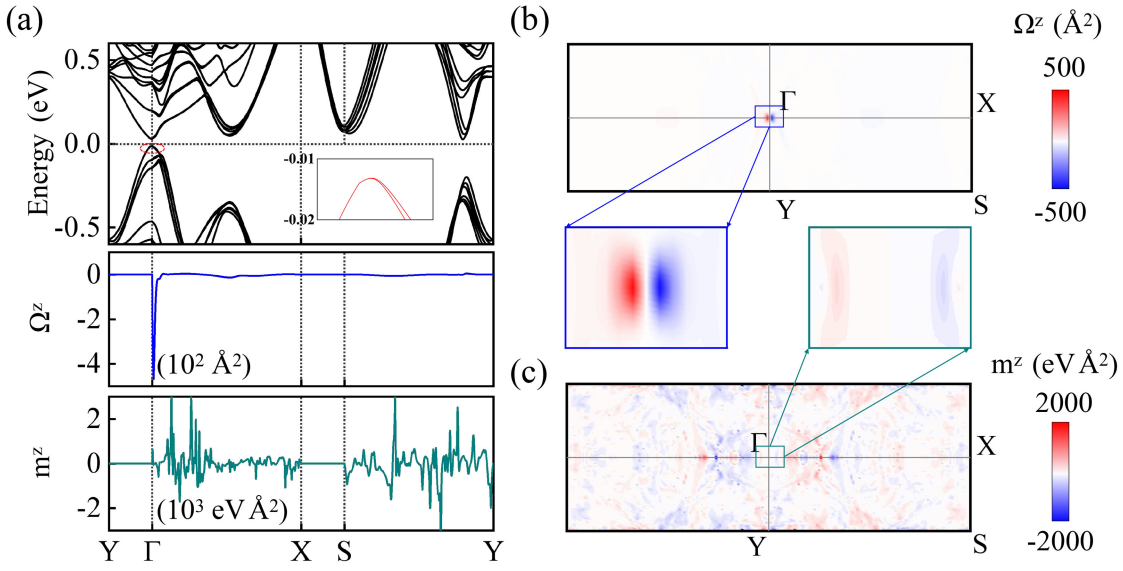

FIG. 2. (a) Band structure (top) for the P_{-1} phase, BC (middle), and OM (bottom) of all occupied bands along the high-symmetry lines in the first BZ. (b),(c) BC and OM as contour maps in the full BZ. The insets show the enlarged plots around Γ.

Berry-phase calculations show that the two stable structures (P_1 and P_{-1}) have significant opposite polarizations of $\pm 1.2 \times 10^{-9}$ C/m. Notably, the electric polarization of trilayer $ZrTe_5$ is 3 orders of magnitude larger than typical values of sliding ferroelectricity in the bilayer of BN [52] and WTe_2 [55] ($\sim 10^{-12}$ C/m), and is even one order of magnitude larger than experimental values of prototypical 2D ferroelectric materials, such as atomic-thick GeS [95,96], SnTe [97], and α-Bi monolayer [98,99] ($\sim 10^{-10}$ C/m).

We further explore the minimum energy path for ferroelectric switching through the nudge-elastic-band method [85]. As the bistable noncentrosymmetric structures of trilayer $ZrTe_5$ are mainly characterized by opposite interlayer sliding of the middle layer, we identify the adiabatic pathway using the sliding displacement λ. As shown in Fig. 1(d) the ferroelectric switching barrier is 2.5 meV/u.c., which is comparable to that of conventional sliding ferroelectrics (9 meV/u.c. for bilayer BN and 0.6 meV/u.c. for bilayer WTe_2) [50,100], indicating the experimental feasibility of polarization reversal via an applied electric field. As shown in Fig. 1(e), the electric polarization depends linearly on λ and changes its sign when λ goes between positive and negative. Moreover, the electric polarization which is along the sliding direction comes from both ionic displacements and electronic charge redistributions (see Sec. VI G in SM [67]), indicating its close relation to the interlayer sliding.

Multilayers and natural cleavage surfaces of $ZrTe_5$.—Similar mechanisms also apply to $ZrTe_5$ multilayers. As an example, we consider the spontaneous sliding of the second subsurface layer near the top surface of $ZrTe_5$ films with their thickness of up to 15 layers [Fig. 1(c)]. Figure 1(f) shows that the optimized sliding distance is around 0.1–0.2 Å and the sliding-induced energy reduction is about 1–7 meV in comparison to the initial multilayer films cutting from the bulk without any sliding or twisting. By scanning the sliding of different layers, we found similar spontaneous $\mathcal{I}$-breaking effects near surfaces, which diminish for inner layers (see Sec. IV in SM [67]). In addition, by examining the sliding effect in bulk with thick unit cells, we found metastable $\mathcal{I}$-breaking phases separated from the centrosymmetric *Cmcm* phase by an activation energy of about 6 meV which requires external stimuli to facilitate the sliding. We, therefore, expect that similar sliding-initiated mechanisms with multiple possible sliding configurations [101,102] are also valid on the natural cleavage (010) surface as well as the bulk of $ZrTe_5$ with the average energy barrier on the order of a few meV, implying a relatively low ferroelectric Curie temperature of tens of kelvin [39].

Ferroelectrically induced BC and OM.—Having clarified the sliding ferroelectricity in trilayer $ZrTe_5$, we further study the unique polarization-dependent BC $\boldsymbol{\Omega}_{\boldsymbol{k}n}$ and OM $\boldsymbol{m}_{\boldsymbol{k}n}^{\mathrm{orb}}$ [103–106], which are given by

$$\boldsymbol{\Omega}_{\boldsymbol{k}n} = \boldsymbol{\nabla}_{\boldsymbol{k}} \times \boldsymbol{A}_{\boldsymbol{k}n} = -\mathrm{Im}\langle \partial_{\boldsymbol{k}} u_{\boldsymbol{k}n}| \times |\partial_{\boldsymbol{k}} u_{\boldsymbol{k}n}\rangle, \quad (1)$$

$$\boldsymbol{m}_{\boldsymbol{k}n}^{\mathrm{orb}} = \frac{e}{2\hbar}\mathrm{Im}\langle \partial_{\boldsymbol{k}} u_{\boldsymbol{k}n}| \times (H_{\boldsymbol{k}} - E_{\boldsymbol{k}n})|\partial_{\boldsymbol{k}} u_{\boldsymbol{k}n}\rangle, \quad (2)$$

where $\boldsymbol{A}_{\boldsymbol{k}n} = i\langle u_{\boldsymbol{k}n}|\partial_{\boldsymbol{k}} u_{\boldsymbol{k}n}\rangle$ is the Berry connection and $E_{\boldsymbol{k}n}$ is the band energy. In 2D, only the out-of-plane components $\Omega_{\boldsymbol{k}n}^{z}$ and $m_{\boldsymbol{k}n}^{\mathrm{orb},z}$ are well defined, which are odd (even) functions of k_x (k_y) enforced by the mirror $\mathcal{M}_x$ and time-reversal $\mathcal{T}$ symmetries (see Table S4 in SM [67]). As shown in Fig. 2(a), the polar P_{-1} phase exhibits a similar band structure as the nonpolar P_0 phase (see Fig. S8 in SM [67]) and has an energy gap of 39 meV. Nevertheless, the

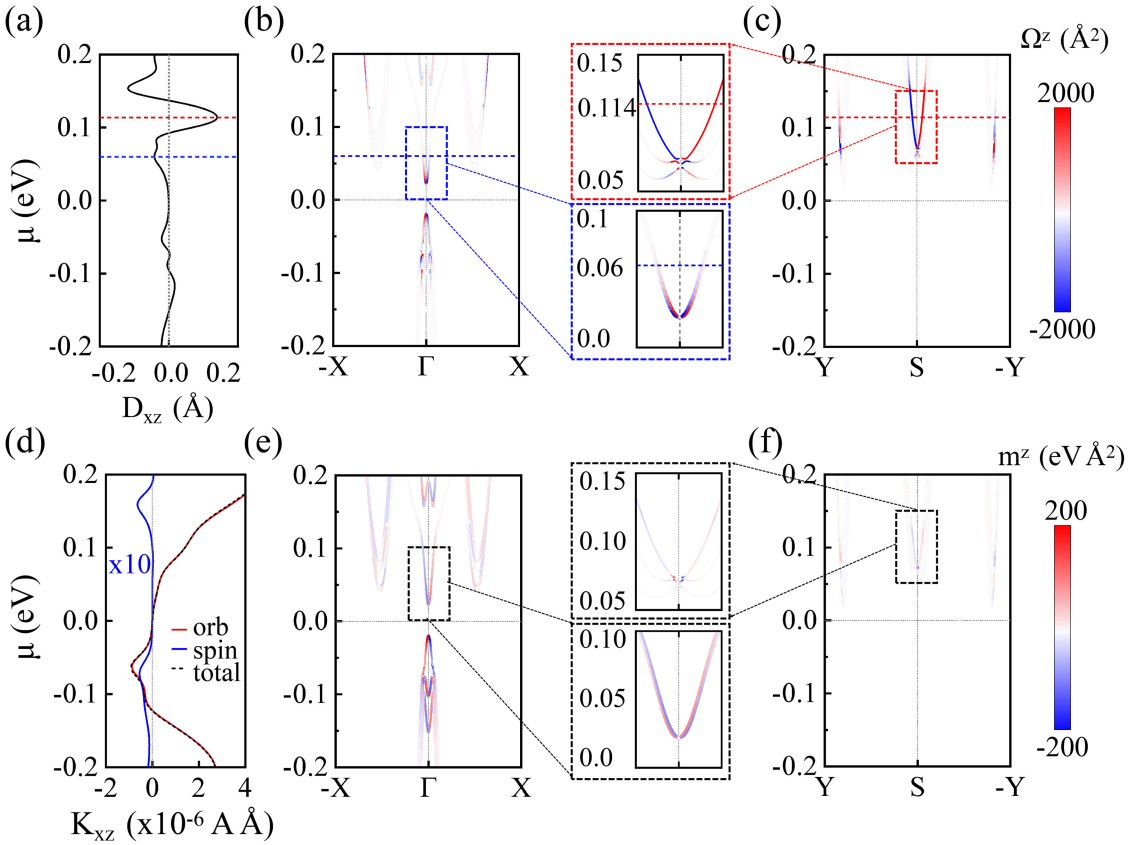

FIG. 3. (a) BCD D_{xz} versus the chemical potential (μ). (b),(c) BC $\Omega^z_{\boldsymbol{k}n}$ for bands along the $((-X)$-Γ-X and Y-S-$(-Y)$ paths. (d) The KME K_{xz} versus μ. (e),(f) OM $\boldsymbol{m}^{\mathrm{orb},z}_{\boldsymbol{k}n}$ for bands along the same k paths. The insets show the enlarged plots around Γ and S.

spontaneous $\mathcal{I}$ breaking in $P_{\pm1}$ results in band splitting at arbitral $\boldsymbol{k}$ points, except for the Γ-Y and X-S paths where the double degeneracy is preserved by $\mathcal{M}_x$, $\mathcal{G}_z$, and $\mathcal{T}$ symmetries. Correspondingly, large $\Omega^z_{\boldsymbol{k}}$ and $m^{\mathrm{orb},z}_{\boldsymbol{k}}$ of all occupied bands appear along the path with band splitting, as shown in the middle and bottom panels of Fig. 2(a). Interestingly, the distribution of $\Omega^z_{\boldsymbol{k}}$ in the full Brillouin zone (BZ) [see Fig. 2(b)] shows a pair of positive and negative BC peaks around Γ, naturally linking to the BC dipole that will be discussed later. In contrast, the $m^{\mathrm{orb},z}_{\boldsymbol{k}}$ distributes more scattered over the entire BZ but still obeys the symmetry constraints. Moreover, the overall sign of BC and OM is reversed by ferroelectric switching between $P_{\pm1}$ with opposite interlayer sliding and electric polarization, revealing a direct coupling between polarization, BC, and OM.

Nonlinear anomalous Hall effect.—The presence of two adjacent and opposite BC peaks around Γ yields a nonzero BC dipole (BCD), which induces the NAHE [69]. Specifically, a second-harmonic transverse current can be generated by an electric field oscillating at a low frequency ω: $j^{2\omega}_a = \chi_{abc} E_b E_c$, where $a, b, c \in \{x, y, z\}$. The nonlinear Hall conductivity associated with the BCD (D_{bd}) is $\chi_{abc} = -\varepsilon_{adc}[e^3\tau/2\hbar^2(1 + i\omega\tau)]D_{bd}$, where τ is the relaxation time and D_{bd} is expressed as

$$D_{bd} = \int_{\mathrm{BZ}} [d\boldsymbol{k}] \sum_n v^n_b \Omega^d_{\boldsymbol{k}n} \left(-\frac{\partial f_0}{\partial E}\right)_{E=E_{\boldsymbol{k}n}}. \tag{3}$$

Here, $v^n_b = (\partial E_{\boldsymbol{k}n}/\partial k_b)$ is the group velocity component for band n, f_0 is the equilibrium occupation factor, and the integral is over the BZ with $[d\boldsymbol{k}] \equiv d^2k/(2\pi)^2$. In the presence of $\mathcal{I}$ symmetry (i.e., the nonpolar P_0 phase), the BCD vanishes completely. Instead, in the polar $P_{\pm1}$ phases, a nonvanishing BCD component D_{xz} is allowed. Because of the derivative of f_0 in Eq. (3), the BCD depends only on quantities around the Fermi surface and is sensitive to the chemical potential μ. Figure 3(a) shows that D_{xz} is zero in the energy gap, while D_{xz} exhibits finite values once μ arises to the conduction bands via electron doping. Especially, there is one significant negative (positive) peak of 0.042 Å (0.139 Å) at $\mu = 0.06$ eV (0.114 eV) near the band edges. These values are comparable with that in monolayer T_d-WTe_2 (~0.11 Å) and strained H-WSe_2 and H-MoS_2 (~0.02 Å) [57,59,61,64,65,107]. Furthermore, the band-resolved BC distribution in Figs. 3(b) and 3(c) indicates that the negative and positive BCD peaks are predominantly contributed by the large $\Omega^z_{\boldsymbol{k}}$ and steep slope (i.e., large v_x) of the slightly split bands around the Γ and S points (see Fig. S12 in SM [67]).

Taking the relaxation time $\tau \sim 57$ fs from experiment [38], we estimate that the nonlinear anomalous Hall conductivity peak in the $\omega \to 0$ limit is $\chi^0_{xxy} = -\chi^0_{yxx} = 1.46 \times 10^{-13}$ A m V^{-2}, which can be detected in experiments. Therefore, one interesting measurement would be the observation of transverse current $j^0_y = 2\chi^0_{yxx}|E_x|^2$ induced by an electric field along the x direction, if one can raise μ via gating [68]. In addition, we found that the ferroelectric switching from P_1 to P_{-1} phase reverses the sign of D_{xz}, while keeping its magnitude intact, thus allowing one to flip the polarity of the transverse current, indicating a remarkable ferroelectric NAHE [58,60].

Kinetic magnetoelectric effect.—Another intriguing effect closely related to the NAHE is the generation of net magnetization by an electrical current, a phenomenon known as KME [108,109]. Within the relaxation-time approximation, the magnetization arises as a linear response to an applied electric field: $M_a = \alpha_{ba}E_b$, where $\alpha_{ba} = [e\tau/(1 - i\omega\tau)]K_{ba}$, with

$$K_{ba} = \int_{\mathrm{BZ}} [d\boldsymbol{k}] \sum_n v^n_b m^a_{\boldsymbol{k}n} \left(-\frac{\partial f_0}{\partial E}\right)_{E=E_{\boldsymbol{k}n}}. \tag{4}$$

It has the same form as Eq. (3) but with the BC replaced by the magnetic moment $\boldsymbol{m}_{\boldsymbol{k}n} = \boldsymbol{m}^{\mathrm{orb}}_{\boldsymbol{k}n} + \boldsymbol{m}^{\mathrm{spin}}_{\boldsymbol{k}n}$, which includes orbital and spin components. Similar to the BCD of polar $P_{\pm 1}$ phases, only the K_{xz} component is allowed due to symmetry constraints, as shown in Fig. 3(d). Noteworthily, K_{xz} originates primarily from the OM with negligible contribution from spin due to the nontrivial topological nature of $ZrTe_5$ (see Sec. VI E in SM [67]) [75]. This is in contrast to 2D inversion layers [110–112] and chiral conductors [92,113] where spin magnetization is predominant or at least comparable with the orbital contribution. As a Fermi surface property, K_{xz} vanishes in the energy gap. Moreover, K_{xz} increases monotonically with electron doping, but exhibits a sign reversal with hole doping, which may be attributed to distinct dispersions of conduction and valence bands. We note that the magnitude of K_{xz} is $\sim 10^{-6}$ AÅ, which is considerable compared to the values of p-doped gyrotropic crystal tellurium (10^{-7} A) [92] and strained monolayer $NbSe_2$ ($\sim 7.63 \times 10^{-6}$ AÅ) [63]. Given the significant K_{xz} in trilayer $ZrTe_5$ with doping, a flow of electric current along the x direction develops a net out-of-plane magnetization M_z. Furthermore, a structural transition between $P_{\pm}$ reverses the direction of M_z.

Physically, NAHE can be understood as the combination of KME and AHE. Specifically, the current-induced magnetization breaks the $\mathcal{T}$ symmetry, leading to the emergence of AHE which generates a transverse current by the electric field in the resulting $\mathcal{T}$-broken system. Actually, $\boldsymbol{\Omega}_{\boldsymbol{k}n}$ and $\boldsymbol{m}_{\boldsymbol{k}n}$ are closely related [92] and exhibit similar distributions in the conduction bands [see Figs. 3(b), 3(c), 3(e), and 3(f)]. Consequently, D_{xz} and K_{xz} are also strongly correlated [64], as we discuss below.

Minimal $k \cdot p$ model analysis.—To explicitly elucidate the underlying mechanism for the sliding-induced BC and OM dipoles, we construct a minimal $k \cdot p$ model H_0 at Γ for P_0 based on symmetry, and introduce the sliding-induced term H_{slide} which drives the system to $P_{\pm}$ phases (see SM for detailed derivations [67]),

$$H_0 = \Delta\tau_z + v_x k_x \tau_x \sigma_z + v_y k_y \tau_y, \tag{5}$$

$$H_{\mathrm{slide}} = \lambda(a_1\tau_x + b_1 k_x \sigma_z + b_2 k_x \tau_z \sigma_z), \tag{6}$$

where $\boldsymbol{\tau}$ and $\boldsymbol{\sigma}$ are two sets of Pauli matrices for the orbital and spin degree of freedom, Δ, $v_{x,y}$, a_1, $b_{1,2}$ are real parameters. We assume that the sliding-induced term depends linearly on λ for simplicity. The energy spectrum of $H_0 + H_{\mathrm{slide}}$ is $E^{\mathrm{sgn}(\mu)}_{\boldsymbol{k}} = \pm\lambda b_1 k_x + \mathrm{sgn}(\mu)h(\boldsymbol{k})$, where $h(\boldsymbol{k}) = \sqrt{(a_1\lambda \mp v_x k_x)^2 + (\Delta + b_2\lambda k_x)^2 + v_y^2 k_y^2}$, and $\mathrm{sgn}(\mu) = \pm$ denotes conduction and valence bands. The bands are split when $\lambda \neq 0$ except for the $k_x = 0$ line, which coincides with the band structure in Fig. 2(a). Moreover, these band splittings give rise to significant BC and OM which together with the band velocity yield the BC and OM dipoles:

$$D_{xz} = \mathrm{sgn}(\mu)\frac{3\Delta b_1}{4\pi\mu^4}(\mu^2 - \Delta^2)\lambda + \mathcal{O}(\lambda^3),$$
$$K^{\mathrm{orb}}_{xz} = -\frac{e\Delta b_1}{2\pi\hbar|\mu|^3}(\mu^2 - \Delta^2)\lambda + \mathcal{O}(\lambda^3), \tag{7}$$

where $|\mu| > \Delta$. One observes that nonzero D_{xz} and K^{orb}_{xz} emerge only if $\lambda \neq 0$, and can be switched by reversing the interlayer sliding. Because of the same symmetry constraint at Γ and S, which form the same little group of C_{2v} (D_{2h}) in the presence (absence) of sliding, a similar analysis also applies at S, which generates additional contributions if one raises μ to reach the Fermi pocket around S. Therefore, our model study indicates a strong coupling between sliding ferroelectricity, NAHE, and KME.

Discussion and conclusion.—An interesting aspect of these intriguing phenomena is that they are also allowed at multilayer films and surfaces of $ZrTe_5$. Although antiferroelectric configurations with antiparallel sliding on opposite surfaces may occur in multilayer films (see SM [67]), the spontaneous sliding on the natural cleavage (010) surface and possible bulk sliding transition driven by various external stimuli, which break $\mathcal{I}$ symmetry, would give rise to the nonlinear Hall currents and out-of-plane magnetization associated with the conductivity χ_{yxx} and KME coefficient α_{xz}, which provides a plausible interpretation for previous experimental observations [39] and renders a challenge for future efforts at experimental detection of surface nonlinear Hall and kinetic magnetoelectric responses [68,75].

In summary, we have proposed the spontaneous $\mathcal{I}$-breaking mechanism in $ZrTe_5$ films which originated from the fantastic structural modification including interlayer sliding and subtle intralayer distortion. We reported the emergence of BC and OM dipoles and unveiled the close connection of associated phenomena, including sliding ferroelectricity, NAHE, and KME. Such sliding-induced ferroelectric switch also adds another ingredient to the intriguing interplay between band topology and nonreciprocal responses already observed in $ZrTe_5$ where more exotic and anomalous behaviors were revealed recently but have yet to be understood very well.

This work is supported by the National Key R&D Program of China (Grant No. 2021YFA1401600), the National Natural Science Foundation of China (Grant No. 12074006), and the China Postdoctoral Science Foundation (Grant No. 2023M740120). H. Z. and W. D. acknowledge support from the Basic Science Center Project of NSFC (Grant No. 52388201), the Ministry of Science and Technology of China, and the Beijing Advanced Innovation Center for Future Chip (ICFC). The computational resources were supported by the high-performance computing platform of Peking University.

E. W. and H. Z. contributed equally to this letter.

*Corresponding author: huaqing.huang@pku.edu.cn

[1] S. Okada, T. Sambongi, and M. Ido, Giant resistivity anomaly in $ZrTe_5$, J. Phys. Soc. Jpn. **49**, 839 (1980).
[2] T. Jones, W. Fuller, T. Wieting, and F. Levy, Thermoelectric power of $HfTe_5$ and $ZrTe_5$, Solid State Commun. **42**, 793 (1982).
[3] B. Fu, H.-W. Wang, and S.-Q. Shen, Dirac polarons and resistivity anomaly in $ZrTe_5$ and $HfTe_5$, Phys. Rev. Lett. **125**, 256601 (2020).
[4] C. Wang, Thermodynamically induced transport anomaly in dilute metals $ZrTe_5$ and $HfTe_5$, Phys. Rev. Lett. **126**, 126601 (2021).
[5] T. Liang, J. J. Lin, Q. Gibson, S. Kushwaha, M. H. Liu, W. D. Wang, H. Y. Xiong, J. A. Sobota, M. Hashimoto, P. S. Kirchmann, Z. X. Shen, R. J. Cava, and N. P. Ong, Anomalous Hall effect in $ZrTe_5$, Nat. Phys. **14**, 451 (2018).
[6] A. Gourgout, M. Leroux, J.-L. Smirr, M. Massoudzadegan, R. P. S. M. Lobo, D. Vignolles, C. Proust, H. Berger, Q. Li, G. Gu, C. C. Homes, A. Akrap, and B. Fauque, Magnetic freeze-out and anomalous Hall effect in $ZrTe_5$, npj Quantum Mater. **7**, 71 (2022).
[7] Z. Sun, Z. Cao, J. Cui, C. Zhu, D. Ma, H. Wang, W. Zhuo, Z. Cheng, Z. Wang, X. Wan, and X. Chen, Large Zeeman splitting induced anomalous Hall effect in $ZrTe_5$, npj Quantum Mater. **5**, 36 (2020).
[8] Y. Liu, H. Wang, H. Fu, J. Ge, Y. Li, C. Xi, J. Zhang, J. Yan, D. Mandrus, B. Yan, and J. Wang, Induced anomalous Hall effect of massive Dirac fermions in $ZrTe_5$ and $HfTe_5$ thin flakes, Phys. Rev. B **103**, L201110 (2021).
[9] P. M. Lozano, G. Cardoso, N. Aryal, D. Nevola, G. Gu, A. Tsvelik, W. Yin, and Q. Li, Anomalous Hall effect at the Lifshitz transition in $ZrTe_5$, Phys. Rev. B **106**, L081124 (2022).
[10] H.-W. Wang, B. Fu, and S.-Q. Shen, Theory of the anomalous Hall effect in the transition metal pentatellurides $ZrTe_5$ and $HfTe_5$, Phys. Rev. B **108**, 045141 (2023).
[11] F. D. Tang, Y. F. Ren, P. P. Wang, R. D. Zhong, J. Schneeloch, S. Y. A. Yang, K. Yang, P. A. Lee, G. D. Gu, Z. H. Qiao, and L. Y. Zhang, Three-dimensional quantum Hall effect and metal-insulator transition in $ZrTe_5$, Nature (London) **569**, 537 (2019).
[12] Y.-X. Wang and Z. Cai, Quantum oscillations and three-dimensional quantum Hall effect in $ZrTe_5$, Phys. Rev. B **107**, 125203 (2023).
[13] S. Galeski *et al.*, Origin of the quasi-quantized Hall effect in $ZrTe_5$, Nat. Commun. **12**, 3197 (2021).
[14] Q. Li, D. E. Kharzeev, C. Zhang, Y. Huang, I. Pletikosić, A. V. Fedorov, R. D. Zhong, J. A. Schneeloch, G. D. Gu, and T. Valla, Chiral magnetic effect in $ZrTe_5$, Nat. Phys. **12**, 550 (2016).
[15] Z. Xie, X. Wei, X. Qiang, Y. Zhang, S. Yan, S. Cao, C. Tian, P. Wang, L. Zhang, G. D. Gu, H. Lu, and J.-H. Chen, Crossover behavior in the magnetoresistance of thin flakes of the topological material $ZrTe_5$, Phys. Rev. B **104**, 125439 (2021).
[16] W. Zhang, P. Wang, B. Skinner, R. Bi, V. Kozii, C.-W. Cho, R. Zhong, J. Schneeloch, D. Yu, G. Gu, L. Fu, X. Wu, and L. Zhang, Observation of a thermoelectric Hall plateau in the extreme quantum limit, Nat. Commun. **11**, 1046 (2020).
[17] J. L. Zhang, C. M. Wang, C. Y. Guo, X. D. Zhu, Y. Zhang, J. Y. Yang, Y. Q. Wang, Z. Qu, L. Pi, H.-Z. Lu, and M. L. Tian, Anomalous thermoelectric effects of $ZrTe_5$ in and beyond the quantum limit, Phys. Rev. Lett. **123**, 196602 (2019).
[18] J. Zhu, C. Lee, F. Mahmood, T. Suzuki, S. Fang, N. Gedik, and J. G. Checkelsky, Comprehensive study of band structure driven thermoelectric response of $ZrTe_5$, Phys. Rev. B **106**, 115105 (2022).
[19] W. Zhang, P. Wang, G. Gu, X. Wu, and L. Zhang, Negative longitudinal magnetothermopower in the topological semimetal $ZrTe_5$, Phys. Rev. B **102**, 115147 (2020).
[20] P. Wang, C.-W. Cho, F. Tang, P. Wang, W. Zhang, M. He, G. Gu, X. Wu, Y. Shao, and L. Zhang, Giant Nernst effect and field-enhanced transversal z_NT in $ZrTe_5$, Phys. Rev. B **103**, 045203 (2021).
[21] B. Xu, L. X. Zhao, P. Marsik, E. Sheveleva, F. Lyzwa, Y. M. Dai, G. F. Chen, X. G. Qiu, and C. Bernhard, Temperature-driven topological phase transition and intermediate Dirac semimetal phase in $ZrTe_5$, Phys. Rev. Lett. **121**, 187401 (2018).
[22] N. L. Nair, P. T. Dumitrescu, S. Channa, S. M. Griffin, J. B. Neaton, A. C. Potter, and J. G. Analytis, Thermodynamic signature of Dirac electrons across a possible topological transition in $ZrTe_5$, Phys. Rev. B **97**, 041111(R) (2018).
[23] I. Mohelsky, J. Wyzula, B. A. Piot, G. D. Gu, Q. Li, A. Akrap, and M. Orlita, Temperature dependence of the

energy band gap in $ZrTe_5$: Implications for the topological phase, Phys. Rev. B **107**, L041202 (2023).
[24] Y. Tian, N. Ghassemi, and J. H. Ross, Jr., Dirac electron behavior and NMR evidence for topological band inversion in $ZrTe_5$, Phys. Rev. B **100**, 165149 (2019).
[25] B. Monserrat and A. Narayan, Unraveling the topology of $ZrTe_5$ by changing temperature, Phys. Rev. Res. **1**, 033181 (2019).
[26] J. Mutch, W.-C. Chen, P. Went, T. Qian, I. Z. Wilson, A. Andreev, C.-C. Chen, and J.-H. Chu, Evidence for a strain-tuned topological phase transition in $ZrTe_5$, Sci. Adv. **5**, eaav9771 (2019).
[27] Z. Tajkov, D. Nagy, K. Kandrai, J. Koltai, L. Oroszlany, P. Sule, Z. E. Horvath, P. Vancso, L. Tapaszto, and P. Nemes-Incze, Revealing the topological phase diagram of $ZrTe_5$ using the complex strain fields of microbubbles, npj Comput. Mater. **8**, 177 (2022).
[28] P. Zhang, R. Noguchi, K. Kuroda, C. Lin, K. Kawaguchi, K. Yaji, A. Harasawa, M. Lippmaa, S. Nie, H. Weng, V. Kandyba, A. Giampietri, A. Barinov, Q. Li, G. D. Gu, S. Shin, and T. Kondo, Observation and control of the weak topological insulator state in $ZrTe_5$, Nat. Commun. **12**, 406 (2021).
[29] C. Vaswani, L.-L. Wang, D. H. Mudiyanselage, Q. Li, P. M. Lozano, G. D. Gu, D. Cheng, B. Song, L. Luo, R. H. J. Kim, C. Huang, Z. Liu, M. Mootz, I. E. Perakis, Y. Yao, K. M. Ho, and J. Wang, Light-driven Raman coherence as a nonthermal route to ultrafast topology switching in a Dirac semimetal, Phys. Rev. X **10**, 021013 (2020).
[30] T. Konstantinova, L. Wu, W.-G. Yin, J. Tao, G. D. Gu, X. J. Wang, J. Yang, I. A. Zaliznyak, and Y. Zhu, Photoinduced Dirac semimetal in $ZrTe_5$, npj Quantum Mater. **5**, 80 (2020).
[31] N. Aryal, X. Jin, Q. Li, M. Liu, A. M. Tsvelik, and W. Yin, Robust and tunable Weyl phases by coherent infrared phonons in $ZrTe_5$, npj Comput. Mater. **8**, 113 (2022).
[32] N. Aryal, X. Jin, Q. Li, A. M. Tsvelik, and W. Yin, Topological phase transition and phonon-space Dirac topology surfaces in $ZrTe_5$, Phys. Rev. Lett. **126**, 016401 (2021).
[33] R. Y. Chen, Z. G. Chen, X.-Y. Song, J. A. Schneeloch, G. D. Gu, F. Wang, and N. L. Wang, Magnetoinfrared spectroscopy of Landau levels and Zeeman splitting of three-dimensional massless Dirac fermions in $ZrTe_5$, Phys. Rev. Lett. **115**, 176404 (2015).
[34] G. Zheng, X. Zhu, Y. Liu, J. Lu, W. Ning, H. Zhang, W. Gao, Y. Han, J. Yang, H. Du, K. Yang, Y. Zhang, and M. Tian, Field-induced topological phase transition from a three-dimensional Weyl semimetal to a two-dimensional massive Dirac metal in $ZrTe_5$, Phys. Rev. B **96**, 121401(R) (2017).
[35] Y. Wang, T. Bömerich, J. Park, H. F. Legg, A. A. Taskin, A. Rosch, and Y. Ando, Nonlinear transport due to magnetic-field-induced flat bands in the nodal-line semimetal $ZrTe_5$, Phys. Rev. Lett. **131**, 146602 (2023).
[36] Y. Choi, J. W. Villanova, and K. Park, Zeeman-splitting-induced topological nodal structure and anomalous Hall conductivity in $ZrTe_5$, Phys. Rev. B **101**, 035105 (2020).
[37] Y. Liu, X. Yuan, C. Zhang, Z. Jin, A. Narayan, C. Luo, Z. Chen, L. Yang, J. Zou, X. Wu, S. Sanvito, Z. Xia, L. Li, Z. Wang, and F. Xiu, Zeeman splitting and dynamical mass generation in Dirac semimetal $ZrTe_5$, Nat. Commun. **7**, 12516 (2016).
[38] Y. Wang, H. F. Legg, T. Bömerich, J. Park, S. Biesenkamp, A. A. Taskin, M. Braden, A. Rosch, and Y. Ando, Gigantic magnetochiral anisotropy in the topological semimetal $ZrTe_5$, Phys. Rev. Lett. **128**, 176602 (2022).
[39] N. Wang, J.-Y. You, A. Wang, X. Zhou, Z. Zhang, S. Lai, H.-J. Tien, T.-R. Chang, Y.-P. Feng, H. Lin, G. Chang, and W.-b. Gao, Non-centrosymmetric topological phase probed by non-linear Hall effect, Natl. Sci. Rev. **11**, nwad103 (2023).
[40] L. Luo, D. Cheng, B. Song, L.-L. Wang, C. Vaswani, P. M. Lozano, G. Gu, C. Huang, R. H. J. Kim, Z. Liu, J.-M. Park, Y. Yao, K. Ho, I. E. Perakis, Q. Li, and J. Wang, A light-induced phononic symmetry switch and giant dissipationless topological photocurrent in $ZrTe_5$, Nat. Mater. **20**, 329 (2021).
[41] Y. Tokura and N. Nagaosa, Nonreciprocal responses from non-centrosymmetric quantum materials, Nat. Commun. **9**, 3740 (2018).
[42] T. Ideue and Y. Iwasa, Symmetry breaking and nonlinear electric transport in van der Waals nanostructures, Annu. Rev. Condens. Matter Phys. **12**, 201 (2021).
[43] J. Lu, G. Zheng, X. Zhu, W. Ning, H. Zhang, J. Yang, H. Du, K. Yang, H. Lu, Y. Zhang, and M. Tian, Thickness-tuned transition of band topology in $ZrTe_5$ nanosheets, Phys. Rev. B **95**, 125135 (2017).
[44] W. Z. Zhuo, B. Lei, C. S. Zhu, Z. L. Sun, J. H. Cui, W. X. Wang, Z. Y. Wang, T. Wu, J. J. Ying, Z. J. Xiang, and X. H. Chen, Thickness-dependent electronic structure in layered $ZrTe_5$ down to the two-dimensional limit, Phys. Rev. B **106**, 085428 (2022).
[45] H. M. Weng, X. Dai, and Z. Fang, Transition-metal pentatelluride $ZrTe_5$ and $HfTe_5$: A paradigm for large-gap quantum spin Hall insulators, Phys. Rev. X **4**, 011002 (2014).
[46] R. Wu, J.-Z. Ma, S.-M. Nie, L.-X. Zhao, X. Huang, J.-X. Yin, B.-B. Fu, P. Richard, G.-F. Chen, Z. Fang, X. Dai, H.-M. Weng, T. Qian, H. Ding, and S. H. Pan, Evidence for topological edge states in a large energy gap near the step edges on the surface of $ZrTe_5$, Phys. Rev. X **6**, 021017 (2016).
[47] X.-B. Li, W.-K. Huang, Y.-Y. Lv, K.-W. Zhang, C.-L. Yang, B.-B. Zhang, Y. B. Chen, S.-H. Yao, J. Zhou, M.-H. Lu, L. Sheng, S.-C. Li, J.-F. Jia, Q.-K. Xue, Y.-F. Chen, and D.-Y. Xing, Experimental observation of topological edge states at the surface step edge of the topological insulator $ZrTe_5$, Phys. Rev. Lett. **116**, 176803 (2016).
[48] G. Qiu, Y. Du, A. Charnas, H. Zhou, S. Jin, Z. Luo, D. Y. Zemlyanov, X. Xu, G. J. Cheng, and P. D. Ye, Observation of optical and electrical in-plane anisotropy in high-mobility few-layer $ZrTe_5$, Nano Lett. **16**, 7364 (2016).
[49] Z. Guo, H. Gu, M. Fang, B. Song, W. Wang, X. Chen, C. Zhang, H. Jiang, L. Wang, and S. Liu, Complete dielectric tensor and giant optical anisotropy in quasi-one-dimensional $ZrTe_5$, ACS Mater. Lett. **3**, 525 (2021).
[50] L. Li and M. Wu, Binary compound bilayer and multilayer with vertical polarizations: Two-dimensional

ferroelectrics, multiferroics, and nanogenerators, ACS Nano **11**, 6382 (2017).
[51] M. V. Stern, Y. Waschitz, W. Cao, I. Nevo, K. Watanabe, T. Taniguchi, E. Sela, M. Urbakh, O. Hod, and M. B. Shalom, Interfacial ferroelectricity by van der Waals sliding, Science **372**, 1462 (2021).
[52] K. Yasuda, X. R. Wang, K. Watanabe, T. Taniguchi, and P. Jarillo-Herrero, Stacking-engineered ferroelectricity in bilayer boron nitride, Science **372**, 1458 (2021).
[53] M. Wu and J. Li, Sliding ferroelectricity in 2D van der Waals materials: Related physics and future opportunities, Proc. Natl. Acad. Sci. U.S.A. **118**, e2115703118 (2021).
[54] D. Zhang, P. Schoenherr, P. Sharma, and J. Seidel, Ferroelectric order in van der Waals layered materials, Nat. Rev. Mater. **8**, 25 (2023).
[55] Z. Fei, W. Zhao, T. A. Palomaki, B. Sun, M. K. Miller, Z. Zhao, J. Yan, X. Xu, and D. H. Cobden, Ferroelectric switching of a two-dimensional metal, Nature (London) **560**, 336 (2018).
[56] S. C. de la Barrera, Q. Cao, Y. Gao, Y. Gao, V. S. Bheemarasetty, J. Yan, D. G. Mandrus, W. Zhu, D. Xiao, and B. M. Hunt, Direct measurement of ferroelectric polarization in a tunable semimetal, Nat. Commun. **12**, 5298 (2021).
[57] Q. Ma, S. Y. Xu, H. T. Shen, D. MacNeill, V. Fatemi, T. R. Chang, A. M. M. Valdivia, S. F. Wu, Z. Z. Du, C. H. Hsu *et al.*, Observation of the nonlinear Hall effect under time-reversal-symmetric conditions, Nature (London) **565**, 337 (2019).
[58] J. Xiao, Y. Wang, H. Wang, C. D. Pemmaraju, S. Wang, P. Muscher, E. J. Sie, C. M. Nyby, T. P. Devereaux, X. Qian, X. Zhang, and A. M. Lindenberg, Berry curvature memory through electrically driven stacking transitions, Nat. Phys. **16**, 1028 (2020).
[59] K. Kang, T. Li, E. Sohn, J. Shan, and K. F. Mak, Nonlinear anomalous Hall effect in few-layer WTe_2, Nat. Mater. **18**, 324 (2019).
[60] H. Wang and X. Qian, Ferroelectric nonlinear anomalous Hall effect in few-layer WTe_2, npj Comput. Mater. **5**, 119 (2019).
[61] S.-Y. Xu, Q. Ma, H. Shen, V. Fatemi, S. Wu, T.-R. Chang, G. Chang, A. M. M. Valdivia, C.-K. Chan, Q. D. Gibson, J. Zhou, Z. Liu, K. Watanabe, T. Taniguchi, H. Lin, R. J. Cava, L. Fu, N. Gedik, and P. Jarillo-Herrero, Electrically switchable berry curvature dipole in the monolayer topological insulator WTe_2, Nat. Phys. **14**, 900 (2018).
[62] X.-G. Ye, H. Liu, P.-F. Zhu, W.-Z. Xu, S. A. Yang, N. Shang, K. Liu, and Z.-M. Liao, Control over berry curvature dipole with electric field in WTe_2, Phys. Rev. Lett. **130**, 016301 (2023).
[63] S. Bhowal and S. Satpathy, Orbital gyrotropic magnetoelectric effect and its strain engineering in monolayer NbX_2, Phys. Rev. B **102**, 201403(R) (2020).
[64] J. Son, K.-H. Kim, Y. H. Ahn, H.-W. Lee, and J. Lee, Strain engineering of the berry curvature dipole and valley magnetization in monolayer MoS_2, Phys. Rev. Lett. **123**, 036806 (2019).
[65] M.-S. Qin, P.-F. Zhu, X.-G. Ye, W.-Z. Xu, Z.-H. Song, J. Liang, K. Liu, and Z.-M. Liao, Strain tunable berry curvature dipole, orbital magnetization and nonlinear Hall effect in WSe_2 monolayer, Chin. Phys. Lett. **38**, 017301 (2021).
[66] A. Zwick, G. Landa, R. Carles, M. Renucci, and A. Kjekshus, Lattice modes in the linear chain compound $ZrTe_5$, Solid State Commun. **44**, 89 (1982).
[67] See Supplemental Material at http://link.aps.org/supplemental/10.1103/PhysRevLett.132.266802 for more details about the derivation of the effective $k \cdot p$ model, first-principles methods, and numerical calculations of bulk, multilayers, and trilayers of $ZrTe_5$, which includes Refs. [33,38,39,45–47,68–94].
[68] S. Singh, J. Kim, K. M. Rabe, and D. Vanderbilt, Engineering Weyl phases and nonlinear Hall effects in T_d-$MoTe_2$, Phys. Rev. Lett. **125**, 046402 (2020).
[69] I. Sodemann and L. Fu, Quantum nonlinear Hall effect induced by Berry curvature dipole in time-reversal invariant materials, Phys. Rev. Lett. **115**, 216806 (2015).
[70] G. L. Bir and G. E. Pikus, *Symmetry and Strain-Induced Effects in Semiconductors* (Wiley, New York, 1974), Vol. 624.
[71] S. Furuseth, L. Brattås, and A. Kjekshus, The crystal structure of $HfTe_5$, Acta Chem. Scand. **27**, 2367 (1973).
[72] C.-X. Liu, H. J. Zhang, B. Yan, X.-L. Qi, T. Frauenheim, X. Dai, Z. Fang, and S.-C. Zhang, Oscillatory crossover from two-dimensional to three-dimensional topological insulators, Phys. Rev. B **81**, 041307(R) (2010).
[73] Y. Zhang, K. He, C.-Z. Chang, C.-L. Song, L.-L. Wang, X. Chen, J.-F. Jia, Z. Fang, X. Dai, W.-Y. Shan, S.-Q. Shen, Q. Niu, X.-L. Qi, S.-C. Zhang, X.-C. Ma, and Q.-K. Xue, Crossover of the three-dimensional topological insulator Bi_2Se_3 to the two-dimensional limit, Nat. Phys. **6**, 584 (2010).
[74] G. Manzoni, L. Gragnaniello, G. Autès, T. Kuhn, A. Sterzi, F. Cilento, M. Zacchigna, V. Enenkel, I. Vobornik, L. Barba *et al.*, Evidence for a strong topological insulator phase in $ZrTe_5$, Phys. Rev. Lett. **117**, 237601 (2016).
[75] K. Osumi, T. Zhang, and S. Murakami, Kinetic magnetoelectric effect in topological insulators, Commun. Phys. **4**, 211 (2021).
[76] R. Resta, Macroscopic polarization in crystalline dielectrics: The geometric phase approach, Rev. Mod. Phys. **66**, 899 (1994).
[77] P. Hosur, Circular photogalvanic effect on topological insulator surfaces: Berry-curvature-dependent response, Phys. Rev. B **83**, 035309 (2011).
[78] F. Nastos and J. E. Sipe, Optical rectification and current injection in unbiased semiconductors, Phys. Rev. B **82**, 235204 (2010).
[79] A. R. Puente-Uriona, S. S. Tsirkin, I. Souza, and J. Ibañez-Azpiroz, *Ab initio* study of the nonlinear optical properties and dc photocurrent of the Weyl semimetal $TaIrTe_4$, Phys. Rev. B **107**, 205204 (2023).
[80] J. Orenstein, J. Moore, T. Morimoto, D. H. Torchinsky, J. W. Harter, and D. Hsieh, Topology and symmetry of quantum materials via nonlinear optical responses, Annu. Rev. Condens. Matter Phys. **12**, 247 (2021).
[81] R. D. King-Smith and D. Vanderbilt, Theory of polarization of crystalline solids, Phys. Rev. B **47**, 1651(R) (1993).

[82] G. Kresse and J. Furthmuller, Efficiency of *ab-initio* total energy calculations for metals and semiconductors using a plane-wave basis set, Comput. Mater. Sci. **6**, 15 (1996).
[83] P. E. Blochl, Projector augmented-wave method, Phys. Rev. B **50**, 17953 (1994).
[84] J. P. Perdew, K. Burke, and M. Ernzerhof, Generalized gradient approximation made simple, Phys. Rev. Lett. **77**, 3865 (1996).
[85] G. Henkelman, B. P. Uberuaga, and H. Jónsson, A climbing image nudged elastic band method for finding saddle points and minimum energy paths, J. Chem. Phys. **113**, 9901 (2000).
[86] J. P. Perdew, A. Ruzsinszky, G. I. Csonka, O. A. Vydrov, G. E. Scuseria, L. A. Constantin, X. Zhou, and K. Burke, Restoring the density-gradient expansion for exchange in solids and surfaces, Phys. Rev. Lett. **100**, 136406 (2008).
[87] S. Grimme, J. Antony, S. Ehrlich, and H. Krieg, A consistent and accurate *ab initio* parametrization of density functional dispersion correction (DFT-D) for the 94 elements H-Pu, J. Chem. Phys. **132**, 154104 (2010).
[88] J. Klimeš, D. R. Bowler, and A. Michaelides, Van der Waals density functionals applied to solids, Phys. Rev. B **83**, 195131 (2011).
[89] N. Marzari and D. Vanderbilt, Maximally localized generalized Wannier functions for composite energy bands, Phys. Rev. B **56**, 12847 (1997).
[90] I. Souza, N. Marzari, and D. Vanderbilt, Maximally localized Wannier functions for entangled energy bands, Phys. Rev. B **65**, 035109 (2001).
[91] S. S. Tsirkin, High performance Wannier interpolation of Berry curvature and related quantities with WannierBerri code, npj Comput. Mater. **7**, 33 (2021).
[92] S. S. Tsirkin, P. A. Puente, and I. Souza, Gyrotropic effects in trigonal tellurium studied from first principles, Phys. Rev. B **97**, 035158 (2018).
[93] A. A. Mostofi, J. R. Yates, Y.-S. Lee, I. Souza, D. Vanderbilt, and N. Marzari, wannier90: A tool for obtaining maximally-localised Wannier functions, Comput. Phys. Commun. **178**, 685 (2008).
[94] Q. Wu, S. Zhang, H.-F. Song, M. Troyer, and A. A. Soluyanov, Wanniertools: An open-source software package for novel topological materials, Comput. Phys. Commun. **224**, 405 (2018).
[95] R. Fei, W. Kang, and L. Yang, Ferroelectricity and phase transitions in monolayer group-IV monochalcogenides, Phys. Rev. Lett. **117**, 097601 (2016).
[96] T. Rangel, B. M. Fregoso, B. S. Mendoza, T. Morimoto, J. E. Moore, and J. B. Neaton, Large bulk photovoltaic effect and spontaneous polarization of single-layer monochalcogenides, Phys. Rev. Lett. **119**, 067402 (2017).
[97] K. Chang, J. W. Liu, H. C. Lin, N. Wang, K. Zhao, A. M. Zhang, F. Jin, Y. Zhong, X. P. Hu, W. H. Duan, Q. M. Zhang, L. Fu, Q. K. Xue, X. Chen, and S. H. Ji, Discovery of robust in-plane ferroelectricity in atomic-thick SnTe, Science **353**, 274 (2016).
[98] J. Gou, H. Bai, X. Zhang, Y. L. Huang, S. Duan, A. Ariando, S. A. Yang, L. Chen, Y. Lu, and A. T. S. Wee, Two-dimensional ferroelectricity in a single-element bismuth monolayer, Nature (London) **617**, 67 (2023).
[99] K.-H. Jin, E. Oh, R. Stania, F. Liu, and H. W. Yeom, Enhanced berry curvature dipole and persistent spin texture in the Bi(110) monolayer, Nano Lett. **21**, 9468 (2021).
[100] Q. Yang, M. Wu, and J. Li, Origin of two-dimensional vertical ferroelectricity in WTe_2 bilayer and multilayer, J. Phys. Chem. Lett. **9**, 7160 (2018).
[101] P. Meng, Y. Wu, R. Bian, E. Pan, B. Dong, X. Zhao, J. Chen, L. Wu, Y. Sun, Q. Fu, Q. Liu, D. Shi, Q. Zhang, Y.-W. Zhang, Z. Liu, and F. Liu, Sliding induced multiple polarization states in two-dimensional ferroelectrics, Nat. Commun. **13**, 7696 (2022).
[102] L. Yang, S. Ding, J. Gao, and M. Wu, Atypical sliding and moiré ferroelectricity in pure multilayer graphene, Phys. Rev. Lett. **131**, 096801 (2023).
[103] R. Resta, Electrical polarization and orbital magnetization: The modern theories, J. Phys. Condens. Matter **22**, 123201 (2010).
[104] T. Thonhauser, Theory of orbital magnetization in solids, Int. J. Mod. Phys. B **25**, 1429 (2011).
[105] D. Xiao, M.-C. Chang, and Q. Niu, Berry phase effects on electronic properties, Rev. Mod. Phys. **82**, 1959 (2010).
[106] D. Ceresoli, T. Thonhauser, D. Vanderbilt, and R. Resta, Orbital magnetization in crystalline solids: Multi-band insulators, Chern insulators, and metals, Phys. Rev. B **74**, 024408 (2006).
[107] J.-S. You, S. Fang, S.-Y. Xu, E. Kaxiras, and T. Low, Berry curvature dipole current in the transition metal dichalcogenides family, Phys. Rev. B **98**, 121109(R) (2018).
[108] L. S. Levitov, Y. V. Nazarov, and G. M. Eliashberg, Magnetoelectric effects in conductors with mirror isomer symmetry, Sov. Phys. JETP **61**, 133 (1985), http://jetp.ras.ru/cgi-bin/dn/e_061_01_0133.pdf.
[109] S. Zhong, J. E. Moore, and I. Souza, Gyrotropic magnetic effect and the magnetic moment on the Fermi surface, Phys. Rev. Lett. **116**, 077201 (2016).
[110] V. M. Edelstein, Spin polarization of conduction electrons induced by electric current in two-dimensional asymmetric electron systems, Solid State Commun. **73**, 233 (1990).
[111] A. G. Aronov and Y. B. Lyanda-Geller, Nuclear electric resonance and orientation of carrier spins by an electric field, JETP Lett. **50**, 398 (1989), http://jetpletters.ru/ps/1132/article_17140.pdf.
[112] S. D. Ganichev, M. Trushin, and J. Schliemann, Spin polarization by current, in *Spintronics Handbook, Second Edition: Spin Transport and Magnetism* (CRC Press, New York, 2019), pp. 317–338.
[113] V. A. Shalygin, A. N. Sofronov, L. E. Vorob'ev, and I. I. Farbshtein, Current-induced spin polarization of holes in tellurium, Phys. Solid State **54**, 2362 (2012).